Observation of Critical-Gradient Behavior in Alfvén-Eigenmode-Induced Fast-Ion Transport

C. S. Collins, W. W. Heidbrink, M. E. Austin, G. J. Kramer, D. C. Pace, C. C. Petty, L. Stagner, M. A. Van Zeeland, R. B. White, Y. B. Zhu, and DIII-D team

Observation of Critical Gradient Behavior In Alfvén Eigenmode Induced Fast-Ion Transport

C. S. Collins,[1, *] W.W. Heidbrink,[1] M.E. Austin,[2] G.J. Kramer,[3] D. C. Pace,[4] C. C.
Petty,[4] L. Stagner,[1] M.A. Van Zeeland,[4] R.B. White,[3] Y. B. Zhu,[1] and the DIII-D team

[1]*University of California-Irvine, Irvine, California 92697, USA*
[2]*University of Texas-Austin, Austin, Texas 78712, USA*
[3]*Princeton Plasma Physics Laboratory, P.O. Box 451, Princeton, New Jersey 08543, USA*
[4]*General Atomics,P.O. Box 85608, San Diego, California 92186-5608, USA*
(Dated: January 21, 2016)

Experiments in the DIII-D tokamak show that fast-ion transport suddenly becomes stiff above a critical threshold in the presence of many overlapping small-amplitude Alfvén eigenmodes (AEs). The threshold is phase-space dependent and occurs when particle orbits become stochastic due to resonances with AEs. Above threshold, equilibrium fast-ion density profiles are unchanged despite increased drive, and intermittent fast-ion losses are observed. Fast-ion Dα (FIDA) spectroscopy indicates radially localized transport of the co-passing population at radii that correspond to the location of mid-core AEs. The observation of stiff fast-ion transport suggests that reduced models can be used to effectively predict alpha profiles, beam ion profiles, and losses to aid in the design of optimized scenarios for future burning plasma devices.

Many plasma systems feature universal transport behavior in which particles, momentum, or energy move in phase space when gradients drive instabilities above a critical threshold. Transport near a critical gradient is of great interest in understanding, for example, substorms in Earth's magnetosphere [1] , or the equilibrium profile limits in fusion plasmas associated with temperature or density gradient driven turbulence [2]. Energetic particle transport studies are particularly relevant for reaching the burning plasma state in a fusion reactor, where a large number of fast ions must be confined for sufficiently long times so that their energy is transferred through collisions to the colder, background plasma. In tokamaks, fast ions are generated by neutral beam injection, ion cyclotron resonance heating, or fusion reactions. However, large gradients in either the fast-ion velocity space or pressure profiles can provide free energy to excite Alfvén eigenmodes (AEs) through wave-particle interactions. The AEs cause fast ions to move away from the core of the plasma, which can affect the current profile, lead to reduced fusion performance, and cause losses that could damage reactor walls [3, 4]. Thus, a comprehensive understanding of the fast-ion transport mechanism and operative regime is imperative.

This Letter presents measurements confirming that multiple, low-amplitude ($\delta B/B \sim \mathcal{O}(10^{-4})$) Alfvén eigenmodes cause stiff fast-ion transport above a phase-space dependent threshold. In the stiff transport regime, fast ions exhibit three elements of ubiquitous self-organized criticality phenomena [5]: (1) a sudden increase in incremental transport at threshold, (2) intermittency, and (3) profile resiliency, i.e., the fast-ion density profiles are virtually unchanged despite increased fast-ion source. This Letter is the first to use a modulation technique to measure incremental fast-ion transport across a critical threshold and the first to report intermittent fast-ion transport in a stiff regime. In addition, although previous work suggested that the critical gradient coincides with the linear stability threshold [6, 7], the novel measurements reported here show conclusively that the transport threshold occurs when the AEs cause particle orbits to become stochastic.

In the experiment, AE activity is created with neutral beam injection during the current ramp phase of a plasma with a low-confinement (L-mode) edge, resulting in a variety of nearly constant frequency Toroidal Alfvén Eigenmodes (TAEs) and frequency sweeping Reverse Shear Alfvén Eigenmodes (RSAEs), which occur near the minimum in the magnetic safety profile ($q_{\min}$). Alfvén activity is measured with the CO_2 interferometer for line-averaged density fluctuations (Fig. 1a-b), electron cyclotron emission (ECE) for electron temperature fluctuations, and external Mirnov coils for magnetic fluctuations. The neutral beam power is scanned from 2-9 MW in multiple discharges. At the lowest power, some AEs are unstable but their amplitude is weak. Above the stability threshold, the amplitude of the AE power spectrum increases approximately linearly with total driving beam power (Fig. 1c), where the amplitude is the sum of the ECE $\Delta T_e/T_e$ power spectrum between the geodesic acoustic and TAE frequencies (typically 60-150 kHz). In DIII-D, the bulk fast-ion distribution function, and thus the AE drive, can be changed by using more perpendicular or more tangential beam injection. In this Letter, only tangential beams are used when total beam power is less than 7 MW, and a mix of tangential and perpendicular beams are used to obtain higher total beam powers.

Particle transport is studied by modulating the fast-ion pressure profile using a single off-axis 0.7 MW neutral beam with peak deposition near mid-radius. The modulated beam period of 50 or 54 ms is selected to produce a clear temporal response in a variety of fast-ion diagnostics (Fig. 2a). Fast-ion density profiles are measured with fast-ion deuterium alpha (FIDA) [8], which records a spectrum of line-integrated, Doppler-shifted light emissions resulting from fast-ion charge exchange collisions with a neutral beam. The FIDA brightness is found by integrating the spectra over a wavelength range which corresponds to a line-of-sight energy range of 21.0-61.3 keV. The FIDA density is found by dividing the brightness by the injected neutral density. Other diagnostics include the solid state neutral particle analyzer (SSNPA) [9], which mea-
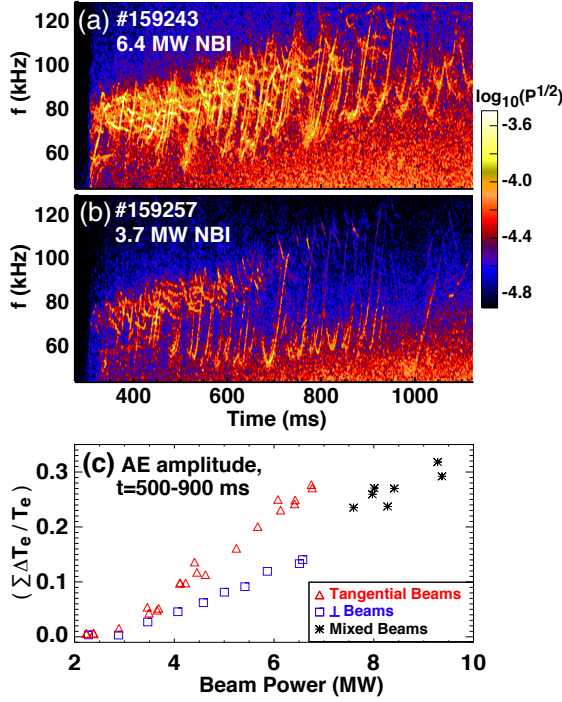
FIG. 1. Example CO_2 interferometer power spectra show multiple RSAEs and TAEs during the current ramp with (a) 6.4 MW and (b) 3.7 MW beam power. (c) Time average of AE amplitude measured by ECE vs total beam power for various combinations of beam geometry.

FIG. 2. Comparison of multiple discharges with varied total beam power. (a) FIDA brightness, (b) SSNPA waveforms with conditional average from t=516-840 ms, and (c) corresponding transport inferred from SSNPA.

sures escaping fast neutrals resulting from charge exchange, the deuterium-deuterium neutron emission rate [10], which is a volumetric proxy for the total number of high energy fast ions, and the fast-ion loss detector [11], which measures fast ions on loss orbits near the machine wall.

Incremental transport is determined from the continuity equation for fast ions. We assume a linear response to the perturbation, so the time evolution of the modulated fast-ion population, $\tilde{n}$, depends on the source, $\tilde{S}$, (the modulated beam), the sink, $\tilde{C}$, (fast-ion thermalization), and transport, $\nabla \cdot \tilde{\Gamma}$ (due to resonant wave-particle interactions with AEs);

$$\frac{\partial \tilde{n}}{\partial t} = \tilde{S} - \tilde{C} - \nabla \cdot \tilde{\Gamma} \qquad (1)$$

This study differs from traditional gas-puffing [12] or heat-pulse propagation experiments [13] in that the source has broad deposition along the injected beam, and the flux, $\tilde{\Gamma}$, is inherently velocity-dependent due to the wave-particle resonance condition. The measured $\tilde{n}$ is a convolution of the fast-ion distribution function and the diagnostic weight function [14], which depends on fast-ion energy, pitch, and the diagnostic geometry.

For this analysis, data (Fig. 2a) are detrended and conditionally averaged over the modulated beam periods between $t = 500 - 900$ ms, where $q_{\min} > 2$. The resulting waveforms (Fig. 2b) become increasingly distorted at high beam powers,
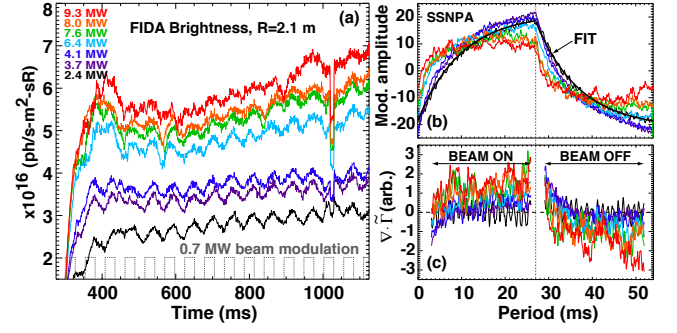
a feature seen in all fast-ion diagnostics that indicates transport. We approximate $\tilde{C} = \tilde{n}/\tau$, where τ depends on both the diagnostic sensitivity and the rate at which fast ions slow down on the background thermal plasma [15]. $\tilde{S}$ and the diagnostic weighting of τ can be found by fitting the density waveform in the low power shot where AEs are weak and transport is negligible, as shown in Fig. 2b. We then use $\tilde{S}$, the measured $\tilde{n}$, and calculated $\tilde{C}$ to find $\nabla \cdot \tilde{\Gamma}$ in discharges with various total neutral beam powers, as shown in Fig. 2c. We have assumed that the calculated source does not change with neutral beam power, since the modulated beam power is unchanged. In reality, $\tilde{S}$ can change as the slowing down time varies when T_e increases with beam heating. (The plasma density is matched with feedback control.) Detailed calculations of the source
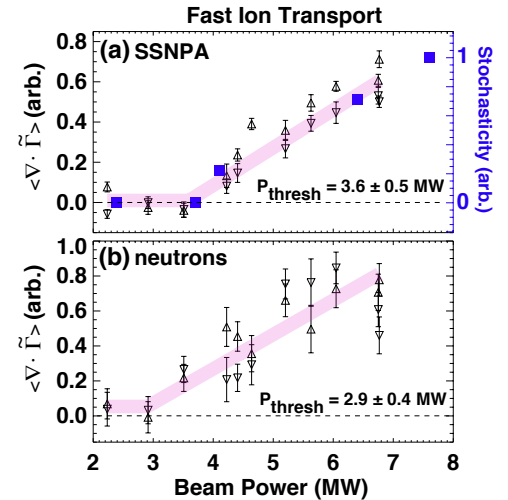

FIG. 3. Time averaged divergence of modulated flux, i.e. transport, for first half (triangles pointing up) and second half (triangles pointing down) of the modulation period. Error bars are standard error of the time average over the half period. The onset of transport corresponds to the theoretical level of stochasticity (solid squares in (a)).
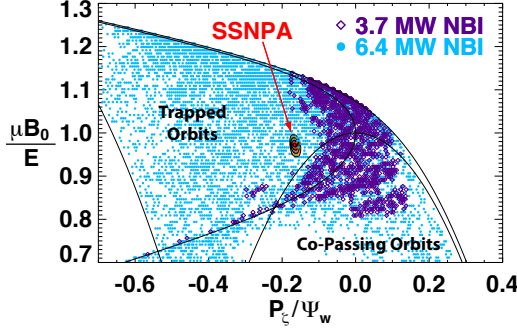
FIG. 4. ORBIT analysis shows that particle orbits in the indicated SSNPA diagnostic region of sensitivity are stochastic in the 6.4 MW case but not stochastic in the 3.7 MW case.

and sink based on classical beam distribution and synthetic diagnostic codes will be presented in future publications, but initial comparisons show only slight differences from the results reported here. In general, Γ can be a time-dependent quantity as fast ions diffuse in space and energy. Here, we take $< \nabla \cdot \tilde{\Gamma} >$ to be the time average of the half period when the beam is either on or off, as indicated in Fig. 2c.

In Fig. 3a, the SSNPA diagnostic shows that transport suddenly begins to increase above a threshold of $P_{thresh} = 3.6 \pm 0.5$ MW beam power, while in Fig. 3b, the neutron emission indicates $P_{thresh} = 2.9 \pm 0.4$ MW. In order to understand what sets the transport threshold, we use a procedure similar to the one in [16] to examine the interaction of the modulated population of particles with the AEs excited in the experiment. The linear ideal magnetohydrodynamic code NOVA [17] is used to compute the eigenmode frequencies and structures for DIII-D discharge #159243 at $t = 790$ ms, which had 6.4 MW of tangential beam injection. The amplitudes of 8 RSAEs and 3 TAEs are scaled to match experimental values based on ECE temperature fluctuation measurements for five discharges in the same power scan at similar timeslices when $q_{min} \sim 2.9$ [18] . The TRANSP code [19] calculates the classical particle distribution function of the modulated beam. Next, the ORBIT algorithm described in [20] is used to determine which portions of fast-ion phase space have good Kolmogorov-Arnold-Moser (KAM) surfaces and which orbits reside in islands and stochastic regions formed by wave-particle resonances. Figure 4 shows the results of this analysis for $E = 70$ keV particles in the portion of phase space diagnosed by the SSNPA. Here, μ is magnetic moment, B_0 is the on-axis magnetic field, P_ζ is the canonical toroidal angular momentum, and Ψ_w is the poloidal magnetic flux at the last closed flux surface. At 3.7 MW, good KAM surfaces are preserved throughout the region diagnosed by the SSNPA, so negligible transport is expected. At 6.4 MW, nearly all surfaces are destroyed, so large transport is expected.

These theoretical results are in good agreement with experiment. In Fig. 3a, the stochasticity, or fraction of SSNPA

phase space with broken surfaces after 15 toroidal transits (4 μs), is plotted beside the experimental data. The experimental threshold for stiff transport coincides with the theoretical points, confirming that the onset of stochasticity is responsible for the jump in transport. Additional observations support this conclusion. (1) The threshold for appreciable transport is lower for diagnostics with broad sensitivity in phase space (such as the neutrons in Fig. 3b) than for diagnostics with narrow sensitivity (such as the SSNPA). Stochastic orbits do exist in lower-power discharges in some portions of phase space, so a diagnostic like the neutron detector that encompasses the entire region of phase space shown in Fig. 4 observes enhanced transport at low power levels. (2) A power scan using perpendicular beams enhances the wave-particle resonances in the trapped portion of phase space. Diagnostics that are sensitive to trapped particles measure a lower power threshold for this perpendicular power scan, while diagnostics that are sensitive to passing particles measure a lower power threshold in the tangential power scan.

The FIDA diagnostic provides profile measurements of the co-passing fast-ion population. Figure 5 shows that transport of the modulated beam particles is localized to the mid-core radii, corresponding to the location of multiple RSAEs. These
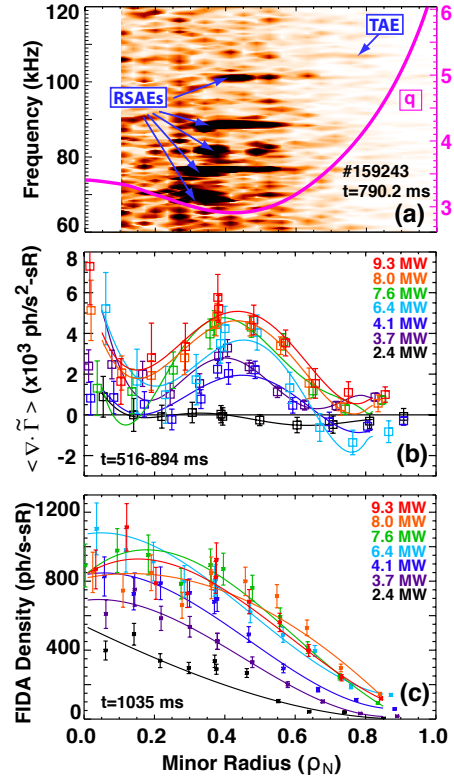

FIG. 5. (a) Radial profile of ECE power spectra at a single timeslice. RSAEs occur at the minimum in q. (b) Fast-ion transport measured with FIDA is localized to the mid-core radii as beam power increases. (c) At increasingly high beam powers, FIDA density profiles at t=1035 ms are unchanged.

observations are consistent with critical gradient behavior in that the modulated beam particles act to perturb the driving gradient, and the particles are consequently redistributed so that the gradient is maintained below the critical value for mode stability. The measured divergence of flux is also non-zero near the magnetic axis, which may be due to the sampling of a portion of trapped fast ions whose large orbit size allows interaction with mid-core AEs. While the gyroradius of a 70 keV fast ion near q_{min} is ~ 2.3 cm, the width of the trapped banana orbit is ~ 40 cm, more than half of the plasma minor radius. At the end of the current ramp, the equilibrium (bulk) FIDA density profiles appear "clamped", with peak density no longer increasing despite increased beam power (Fig. 5c).

The fast-ion losses at the modulated beam frequency also suddenly increase above a threshold in driving beam power. In addition, the fast-ion losses exhibit larger, more frequent transient bursts as beam power increases, appearing as a growing tail of the probability distribution function of the intermittency (Fig. 6). Here, intermittency is defined as the raw data divided by the smoothed data (sampled at 1 MHz and boxcar averaged with 0.1 ms window). While the total AE power decreases in time through the current ramp, the types of AEs evolve (as can be seen in the spectra in Fig. 1a and 1b), with strong, simultaneous RSAEs and TAEs generally occurring from 700-800 ms, corresponding to a peak in the intermittent activity. In theory, if many overlapping modes are present, particle diffusion can occur over a larger portion of phase space, leading to an avalanche of global redistribution and losses [21]. While an absolute calibration of losses to assess the degree of wall heating in the existing experiment is not available, it is conceivable that the combination of AE-induced diffusive and intermittent losses could be unacceptable in future burning plasma devices, and further characterization of the operative regime for this loss mechanism is needed.

For predictive studies of AE induced transport, a fully self-consistent numerical treatment would evolve the AE structures, amplitudes, and frequencies with the fast-ion distribution function and equilibrium plasma profiles. Although recent progress has been impressive [22, 23], this approach is very expensive computationally. As an alternative, reduced models aim to make computation efficient by avoiding detailed nonlinear calculations of wave-particle resonances and saturated mode amplitudes, but accuracy must be evaluated through experimental validation. While the isotropic, fusion produced alpha particle distribution function in a thermonuclear plasma such as ITER cannot be produced in present day devices where neutral beams drive anisotropic fast ions, it is expected that many small amplitude AEs will similarly be present in ITER [24]. The measurements of diffusive and intermittent transport presented in this Letter can be used to quantitatively validate AE critical gradient "stiff" transport models, giving greater confidence when applying the numerical tool to ITER.

In recent work, the relaxed fast-ion pressure profile is calculated by assuming that AE induced fast-ion transport is stiff above either the AE linear stability threshold [7] or a micro-
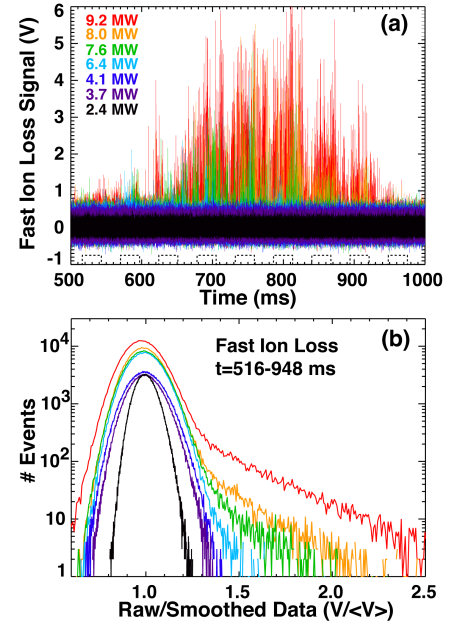

FIG. 6. (a) Spikes in the FILD data increase with beam power, quantified in (b) as a skewed tail in the event distribution function of the raw signal divided by the 0.1 ms running average.

turbulent threshold [25]. The experimental results presented here suggest that the use of a linear stability threshold yields predictions that are unrealistically pessimistic. Successful reduced models must incorporate an algorithm that evaluates the threshold for orbit stochasticity and accounts for transport thresholds that differ in phase space, since eigenmodes can perturb only a portion of phase space and leave other parts unaffected.

In summary, experimental evidence for Alfvén eigenmode induced fast-ion transport is consistent with critical-gradient behavior. Fast-ion transport suddenly increases above a threshold in driving beam power, and the threshold differs between various fast-ion diagnostics. ORBIT simulations indicate that the threshold occurs when the region of phase space measured by the diagnostic becomes stochastic. Above the phase-space dependent threshold, fast-ion transport becomes stiff, where an incremental change in drive results in a proportional increase in transport. In this regime, multiple small amplitude RSAEs and TAEs with many wave-particle resonances exist, and transport results in virtually unchanged equilibrium fast-ion density profiles despite increased drive, along with increased intermittent spikes in the fast-ion losses.

`https://fusion.gat.com/global/D3D_DMP.`

------

* collinscs@fusion.gat.com

[1] A. Klimas, J. Valdivia, D. Vassiliadis, D. Baker, M. Hesse, and J. Takalo, J. Geophys. Res. **105**, 18765 (2000).

[2] E. Doyle, W. Houlberg, Y. Kamada, V. Mukhovatov, *et al.*, Nucl. Fusion **47**, S18 (2007).

[3] W. W. Heidbrink, Phys. Plasmas **15**, 055501 (2008).

[4] N. N. Gorelenkov, S. D. Pinches, and K. Toi, Nucl. Fusion **54**, 125001 (2014).

[5] P. H. Diamond and T. S. Hahm, Phys. Plasmas **2**, 3640 (1995).

[6] W. W. Heidbrink, M. A. Van Zeeland, M. E. Austin, E. M. Bass, K. Ghantous, N. N. Gorelenkov, B. A. Grierson, D. A. Spong, and B. J. Tobias, Nucl. Fusion **53**, 093006 (2013).

[7] K. Ghantous, N. N. Gorelenkov, H. L. Berk, W. W. Heidbrink, and M. A. Van Zeeland, Phys. Plasmas **19**, 092511 (2012).

[8] C. M. Muscatello, W. W. Heidbrink, D. Taussig, and K. H. Burrell, Rev. Sci. Instrum. **81**, 10D316 (2010).

[9] Y. B. Zhu, A. Bortolon, W. W. Heidbrink, S. L. Celle, and A. L. Roquemore, Rev. Sci. Instrum. **83**, 10D304 (2012).

[10] W. W. Heidbrink, P. L. Taylor, and J. A. Phillips, Rev. Sci. Instrum. **68**, 536 (1997).

[11] R. K. Fisher, D. C. Pace, M. García-Munoz, *et al.*, Rev. Sci. Instrum. **81**, 10D307 (2010).

[12] H. Takenaga, K. Nagashima, A. Sakasai, T. Oikawa, and T. Fujita, Plasma Phys. Control. Fusion **40**, 183 (1998).

[13] J. Hillesheim, J. DeBoo, W. Peebles, T. Carter, G. Wang, *et al.*, Phys. Rev. Lett. **110**, 045003 (2013).

[14] W. W. Heidbrink, Y. Luo, K. H. Burrell, R. W. Harvey, R. I. Pinsker, and E. Ruskov, Plasma Phys. Control. Fusion **49**, 1457 (2007).

[15] J. D. Strachan, P. L. Colestock, S. L. Davis, D. Eames, *et al.*, Nucl. Fusion **21**, 67 (1981).

[16] R. B. White, N. Gorelenkov, W. W. Heidbrink, and M. A. VanZeeland, Plasma Phys. Control. Fusion **52**, 045012 (2010).

[17] N. N. Gorelenkov, C. Z. Cheng, and G. Fu, Phys. Plasmas **6**, 2802 (1999).

[18] M. A. Van Zeeland, G. J. Kramer, M. E. Austin, R. L. Boivin, W. W. Heidbrink, *et al.*, prl **97**, 135001 (2006).

[19] A. Pankin, D. McCune, R. Andre, G. Bateman, and A. Kritz, Comp. Phys. Comm. **159**, 157 (2004).

[20] R. B. White, Commun. Nonlinear Sci. Numer. Simul. **17**, 2200 (2012).

[21] H. L. Berk, B. N. Breizman, J. Fitzpatrick, and H. V. Wong, Nucl. Fusion **35**, 1661 (1995).

[22] Y. Todo, M. A. Van Zeeland, A. Bierwage, and W. W. Heidbrink, Nucl. Fusion **54**, 104012 (2014).

[23] M. Schneller, P. Lauber, R. Bilato, M. Garcia-Munoz, M. Brudgam, S. Gunter, and the ASDEX Upgrade Team, Nucl. Fusion **53**, 123003 (2013).

[24] G. Vlad, S. Briguglio, G. Fogaccia, F. Zonca, and M. Schneider, Nucl. Fusion **46**, 1 (2006).

[25] R. E. Waltz and E. M. Bass, Nucl. Fusion **54**, 104006 (2014).